Preprint Title	Heat-induced transformation of nickel-coated polycrystalline diamond film studied in situ by XPS and NEXAFS
Authors	Olga Sedelnikova, Yuliya Fedoseeva, Dmitriy Gorodetskiy, Yuriy Palyanov, Elena Shlyakhova, Eugene Maksimovskiy, Anna Makarova, Lyubov Bulusheva and Alexander Okotrub
Publication Date	05 März 2025
Article Type	Full Research Paper
Supporting Information File 1	SM_BJNANO.docx; 2.3 MB
ORCID® iDs	Olga Sedelnikova - https://orcid.org/0000-0002-0491-3208; Yuliya Fedoseeva - https://orcid.org/0000-0003-1681-1708; Dmitriy Gorodetskiy - https://orcid.org/0000-0002-3446-7480; Eugene Maksimovskiy - https://orcid.org/0000-0002-1555-2719; Anna Makarova - https://orcid.org/0000-0002-5603-5566; Lyubov Bulusheva - https://orcid.org/0000-0003-0039-2422; Alexander Okotrub - https://orcid.org/0000-0001-9607-911X

Heat-induced transformation of nickel-coated polycrystalline diamond film studied in situ by XPS and NEXAFS

O. V. Sedelnikova*[‡1], Y. V. Fedoseeva[‡1], D. V. Gorodetskiy[1], Y. N. Palyanov,[2] E.V. Shlyakhova,[1] E. A. Maksimovskiy,[1] A. A. Makarova[§3], L. G. Bulusheva,[1] and A. V. Okotrub[1]

Address: [1]Nikolaev Institute of Inorganic Chemistry, SB RAS, 630090 Novosibirsk, Russia; [2]Sobolev Institute of Geology and Mineralogy SB RAS, 630090 Novosibirsk, Russia, and [3]Physical Chemistry, Institute of Chemistry and Biochemistry, Free University of Berlin, 14195 Berlin, Germany

Email: Olga V. Sedelnikova – sedelnikova@niic.nsc.ru

* Corresponding author

‡ Equal contributors

§ Present address: Helmholtz-Zentrum Berlin für Materialien und Energie, 14109 Berlin, Germany

Abstract

Controlling the high-temperature graphitization of diamond surface is important for many applications that require the formation of thin conductive electrodes on dielectric substrate. Transition metal catalysts can facilitate the graphitization process. In this

work, a polycrystalline diamond films with mixed grain orientation, as well as a synthetic single crystal diamond with a polished (110) face, were covered with a nickel thin film deposited by thermal evaporation method. The effect of nickel on the chemical state of diamond surfaces after high vacuum annealing at a temperature of about 1100 °C has been studied in situ using synchrotron based X-ray photoelectron spectroscopy and near-edge X-ray absorption fine structure spectroscopy (NEXAFS). Differences in the morphology and structure of annealed polycrystalline diamond films with and without nickel were evidenced using scanning electron microscopy and Raman spectroscopy. Nickel-coated polycrystalline and single crystal diamond surfaces were found to be more prone to transformation into sp^2-hybridized carbon compared to their nickel-free counterparts. XPS data revealed the formation of a thin graphite-like film with low-ordered atomic structure on the surface of the nickel-coated polycrystalline film. The chemical state of sp^2-hybridized carbon atoms was found to be insensitive to the face orientation of the diamond micro-sized crystallites; however, the layer defectiveness increased in areas with fine-dispersed crystallites. The angular dependence of NEXAFS spectra at the C K-edge of annealed nickel-coated (110) face of single crystal diamond discovered the vertical orientation of sp^2-hybridized carbon layers relative to the diamond surface.

Keywords

Polycrystalline diamond film, single-crystal diamond; graphitization; nickel coating; X-ray photoelectron spectroscopy; near-edge X-ray absorption fine structure spectroscopy

Introduction

Diamond and graphite, both composed entirely of carbon atoms, exhibit vastly different properties due to their distinct atomic structures. Diamond is a wide-bandgap semiconductor, which makes it resistant to high voltages and ionizing radiation. In contrast, graphitic materials demonstrate excellent electrical conductivity. This divergence in physical properties has encouraged significant interest in producing hybrid materials that combines these two forms of carbon [1-3]. In particular, such graphene-on-diamond heterostructures have been showed to be attractive for power electronics [4,5], microelectronic devices [6,7], and detectors [7,8].

At room temperature and atmospheric pressure, carbon in sp^3 hybridization is a metastable material. A significant activation barrier hampers its relaxation into sp^2 graphitic carbon, and this transformation occurs during vacuum heating in the temperature range of 1500–1800 °C [9]. According to the molecular dynamics simulations, graphitization of non-terminated diamond surface is initiated at 750 °C, the temperature of about 1500°C is needed for the formation of extended graphene-like layers, and temperatures higher than 2000 °C are required for the complete conversion of the diamond (111) surface to graphitic layers [10, 11]. Thermal stability of diamond crystals depends on the crystallographic orientation of their faces [12, 13]. In particular, the (100) face exhibits greater resistance to annealing compared to the (111) face [10, 13, 14], and the (110) face has proven to be the most unstable when exposed to high temperatures [14, 15].

The coating of the diamond surface with a metal catalyst has been explored to reduce the temperatures required for the initiation of the graphitization process. Nickel [16-23], iron [25-27], copper [28,29], gallium [30], and molybdenum [31] allow the fabrication of graphene-on-diamond heterostructures by annealing. Among them, nickel attracts

specific attention due its lattice parameter closely matching that of diamond. Both single-crystal diamond (SCD) [18, 21-23] and nanocrystalline diamond (NCD) [17, 19, 20] films were subjected under Ni-assisted graphitization. The transformation of SCD surface into graphene requires annealing at temperatures above 800 °C [23]. The mechanism of the catalytic process of converting diamond into graphite involves the release of carbon atoms from the diamond surface, counter-diffusion of carbon and nickel atoms at the Ni-diamond interface [17, 21]. Excess carbon atoms dissolved in the nickel lattice leads to the formation of continuous layers of sp^2-hybridized carbon on the top or side surfaces of Ni particles and etching of the diamond surface under them. Comparing the morphology of the Ni-coated SCDs annealed under similar conditions revealed the anisotropic nature of both the diamond etching [32, 33] and the graphitization of diamond surface [21]. In particular, the (111) face was found to be resistant to etching, while nickel nanoparticles penetrated below the diamond surface, creating pits that were partially filled with graphite [21].

A major drawback of fabricating graphene-on-diamond heterostructures using SCD wafers is their high cost. In this regard, polycrystalline diamond (PCD) films provide an excellent alternative to SCDs, as they exhibit properties similar to those of SCDs and can be obtained on large-area substrates using a more accessible plasma-enhanced chemical vapor deposition (PE CVD) method. The annealing of NCD films in the presence of Ni catalyst has been explored recently [17, 19, 20]. It was shown that graphitization of Ni-coated NCD films begins at relatively lower temperature of about 500 °C compared to the Ni-coated SCD [19]. Such a significant decrease in the temperature at which graphitization starts is due to the presence of multiple grain boundaries, along which the diffusion of Ni atoms takes place, facilitating the graphitization process [34]. On the other hand, the nano-granular diamond films prevent the formation of a large-scale graphene-like coating. A possible solution to this

4

problem is to anneal microcrystalline samples; however, there is no research on the graphitization of such PCD films in the presence of nickel catalyst.

To fill this gap, we focused on the changes in the surface state of the Ni-coated PCD film composed of micron-sized crystallites with (110) and (111) faces during high vacuum annealing at a temperature of about 1100 °C. In situ X-ray photoelectron spectroscopy (XPS) and near-edge X-ray absorption fine structure (NEXAFS) spectroscopy investigations of heat-induced transformation of the surface of bare and Ni-coated PCD films were conducted at the experimental station of the Russian−German Beamline using the BESSY II synchrotron radiation facility. The annealed films were not contact to air before XPS and NEXAFS experiments. However, after synchrotron measurements, they were exposed to air and further analyzed using scanning electron microscopy (SEM) and Raman spectroscopy. Additionally, angle-resolved NEXAFS spectra were measured for the Ni-coated SCD with a polished (110) surface annealed under approximately the same conditions to reveal the orientation of the formed graphitic layers. The obtained results allowed us to study in detail the morphology of the graphitized layer formed during annealing in the presence of nickel on the surface of the PCD film, and to determine the texture of the graphitized layers relative to the (110) diamond face of SCD.

Results and Discussion

Surface transformation of bare and nickel-coated polycrystalline diamond film under high vacuum annealing

The PCD film was produced by PE CVD method using acetone $(CH_3)_2CO$ and hydrogen (H_2) as the precursor gases for plasma [35]. The film consists of crystallites

with non-uniform geometry, dimensions, and orientation (Figure S1a-c). The large diamond micro-sized crystallites, measuring about 100 μm, have a complex shape of cuboctahedron with facets that have straight and acute angles. The electron backscatter diffraction (EBSD) analysis detected the (110) and (111) crystallographic planes of the largest grains located on the surface the PCD film (Figure S1b). The mapping did not show regions with the (100) orientation, although cubic faces are visible in SEM images. The signal from these faces is probably weakened due to the tilt of the crystallites and the rough PCD film. Various growth defects are present on the diamond faces, including pits, cracks, steps, and protrusions. The secondary nucleation of diamond caused the formation of submicron-sized diamond grains and smoothing of the shape of large crystals. Raman spectroscopy revealed a high crystalline quality in PCD film at micron scale (Figure S2). Thermal evaporation of nickel and its deposition on the PCD film surface resulted in the formation of a uniform metallic layer with a thickness of about 40 nm (Figure S1d). The bare PCD film and that with nickel coating (denoted Ni-PCD) were placed on the same holder and annealed simultaneously in the vacuum chamber of the RGL-PES end-station of BESSY at 1100 °C for 15 min. After annealing PCD and Ni-PCD films were cooled to room temperature without contact with air and examined in situ using synchrotron radiation NEXAFS and XPS spectroscopies. The changes in the chemical state of the surface of PCD and Ni-PCD films as a result of annealing were examined.

The NEXAFS C K-edge spectra were recorded simultaneously in total electron yield (TEY) and Auger electron yield (AEY) modes to probe the volume (10 nm) and the surface (3 nm) of the films, respectively (Figure 1). The C K-edge spectra of the annealed samples show the sharp peak at 289.3 eV assigned to the 1s→σ* electron transition within the sp^3–hybridized carbon atoms in the diamond ($σ*(sp^3)$) and a wide dip at 302.2 eV corresponding to a second absolute gap in the diamond band structure

6

[36]. In the TEY spectra of both PCD and Ni-PCD films, the aforementioned spectral features are well pronounced, that indicates the preservation of the ordered crystalline structure of diamond in the bulk of the film after annealing (Figure 1a). In the AEY spectra of both films, the smoother shape of the $\sigma^*(sp^3)$ resonance and the shallower dip refer to the presence of structural disorders on the surface of diamond films (Figure 1b). The amount of these disorders in Ni-PCD is higher than that in PCD. This result confirms previous findings that the metal catalyst induces the formation of disordered carbon on the diamond surface during annealing [17, 19, 23, 37]. All spectra also show a low-intensity feature at 285.4 eV corresponding to the 1s→ π^* electron transition within sp^2-hybridized carbon species ($\pi^*(sp^2)$). This peak is more intense in the AEY spectra than in the TEY spectra, meaning that the film surface consists of carbon atoms in sp^2-hybridized states. The $\pi^*(sp^2)$ peak in the spectra of the annealed Ni-PCD film has much higher intensity than that in the spectra of the annealed PCD film. Based on this observation, we can conclude that nickel promotes the conversion of the diamond film surface into a sp^2-carbon coating upon annealing. This result confirms the previously reported findings, which demonstrated the catalytic role of nickel in the reconstruction of diamond surface [16-23]. Based on electron microscopy and Raman spectroscopy data, the authors claimed that graphite or graphene-like layers are products of the diamond annealing process.

The intensity ratio of $\pi^*(sp^2)$- and $\sigma^*(sp^2)$-resonances in NEXAFS C K-spectra of the annealed samples can be used for qualitative assessment of structural perfection in graphitic-like material. Graphite and graphene have a high degree of local crystallinity (i.e., a high ordering of carbon atoms in the honeycomb network) and their C K-edge spectra contain a narrow and high intensive $\pi^*(sp^2)$-resonance [38, 39]. However, the rather low intensity of the $\pi^*(sp^2)$-resonance in the spectrum of the annealed Ni-PCD film indicates that annealing of polycrystalline films on average leads to the formation

7

of structurally highly disordered forms of sp^2 carbon layers. The AEY spectra of the annealed PCD and Ni-PCD films exhibit an additional pronounced feature at about 284.0 eV, which can be also assigned to π*(sp^2)-resonance and associated with the presence of large aromatic fragments on the surface of both annealed films [40]. Moreover, this peak overlaps with the characteristic C K-edge features of transition metal carbides; therefore, it can also be attributed to the presence of Ni–C states in the annealed Ni-PCD film [41].
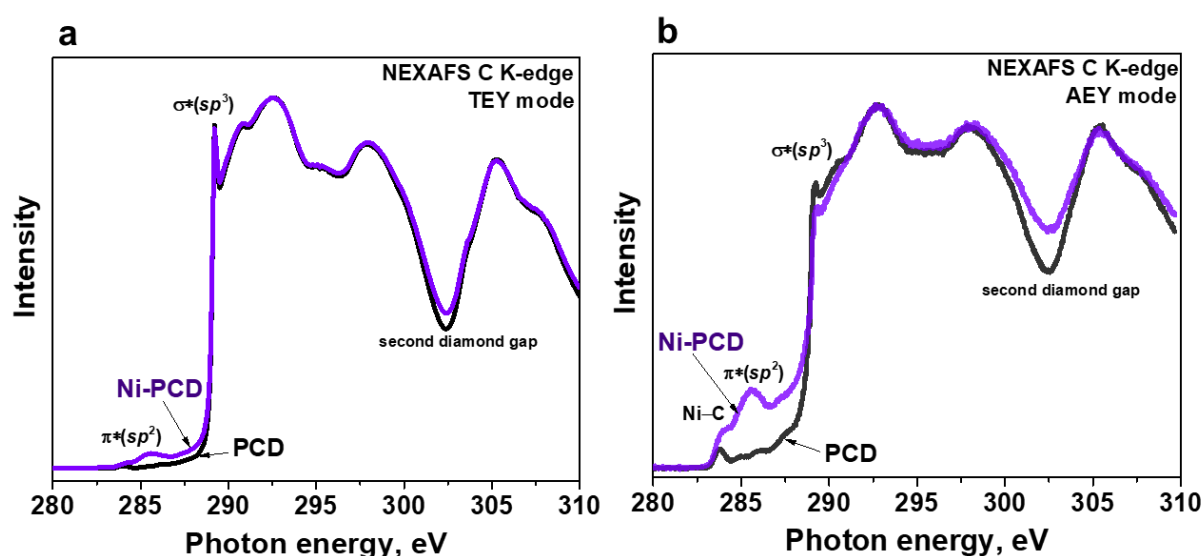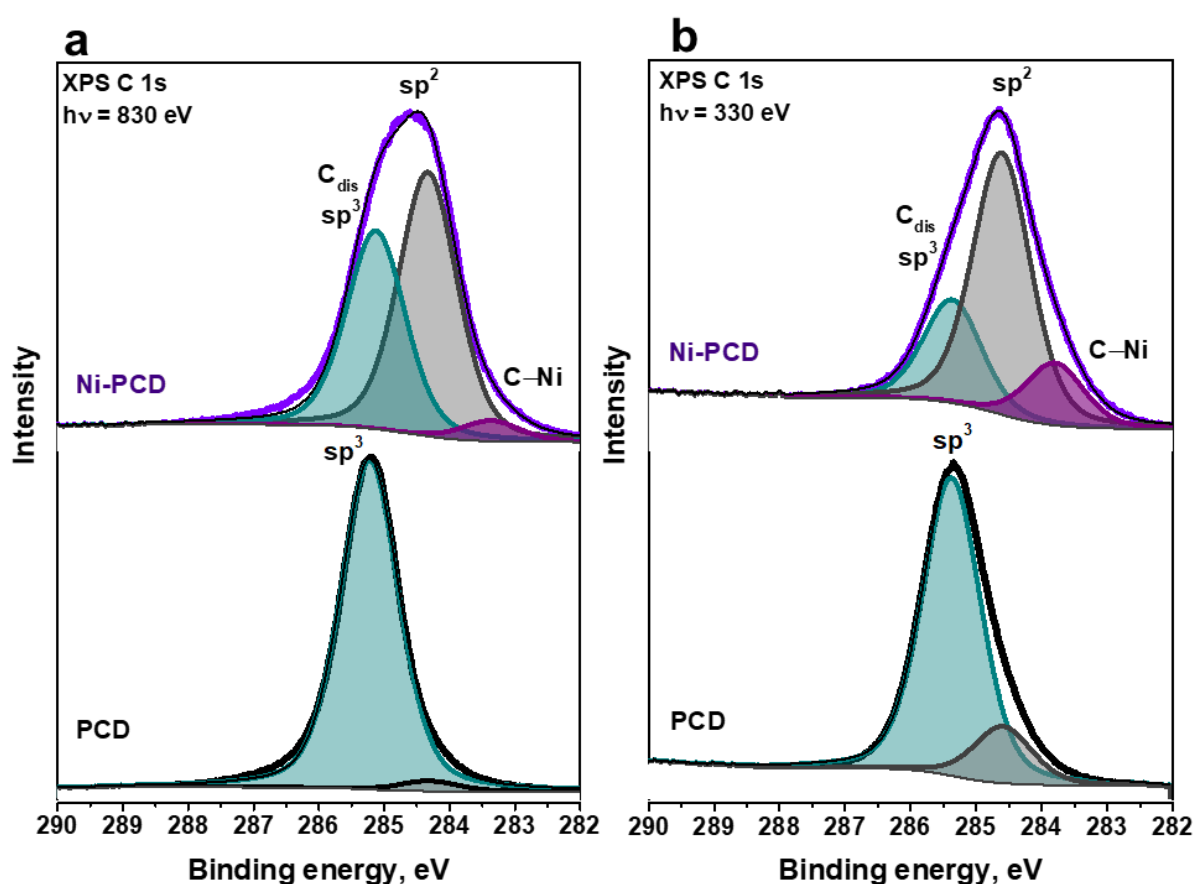

Figure 1: NEXAFS C K-edge spectra of PCD and Ni-PCD films after high vacuum annealing at 1100 °C, measured in a) TEY mode and b) AEY mode.

Survey XPS spectra of the annealed samples showed a strong C 1s line at ~285 eV and a weak Ni 3p peak at ~67 eV only for the Ni-PCD film (Figure S3). The oxygen and other elements were not detected in the surface of the samples. The low surface concentration of nickel (0.1 at%) could be associated with the heat-induced reorganization of Ni layer into particles, which can penetrate into diamond substrate due to counter-diffusion of carbon and nickel [21]. The immersing of metal particles into diamond was discussed in detail in previous works [26, 27]. Moreover, a small

amount of disordered carbon can be deposited on the surface of Ni particles due to segregation of dissolved carbon during cooling. These metal particles are more probably coated with sp^2-carbon shells.

The XPS C 1s spectra were measured upon excitation by photons with energies of 830 and 330 eV to probe different depths of the samples' surfaces after annealing (Figure 2). In these cases, the inelastic mean free path for electrons emitted from C 1s level in diamond is about 1.0 nm (probing depth of 3 nm) for 830 eV and 0.7 nm (probing depth of 2.1 nm) for 330 eV, respectively [42]. The C 1s spectrum of PCD after high vacuum annealing was fitted with two components. The dominant peak at 285.2 eV is assigned to sp^3-hybridized carbon atoms in diamond crystals. Additionally, there is a tiny peak located at 284.3 eV corresponding to sp^2-hybridized carbon atoms. The relative area of this sp^2-peak is 3% in the spectrum measured at 830 eV, and becomes significantly large (16%) as the photon excitation energy decreases to 330 eV. The rather small amount of sp^2 carbon in the 2 nm thick surface layer indicates that the temperature and duration of the annealing process were not sufficient to achieve significant graphitization of the PCD surface without a nickel layer. In contrast, an intensive sp^2-carbon component is observed in the C 1s spectra of Ni-PCD, confirming that the diamond surface in the presence of nickel catalyst transforms to sp^2-hybridized carbon more readily. For excitation of 830 eV, the sp^2 peak is quite broad (1.1 eV) compared to that in the spectrum of a highly ordered graphite crystal (0.6 eV) [39]. The reason for this is the high density of defects in the carbon layer formed on the Ni-PCD surface during annealing. In the spectrum of the annealed Ni-PCD surface, the peak at 285.2 eV can be assigned to diamond sp^3-states similar to that in the initial diamond, however highly disordered sp^2 carbon states (C_{dis}) can also give rise to this peak. According to a recent XPS study of the graphitization process of Ni-coated NCD films, a disordered carbon was found to form on the nickel surface, which then partially transformed into

a graphitic phase at higher temperatures [19]. Moreover, the spectra of the annealed Ni-PCD film demonstrate an additional peak at low binding energy of 283.3 eV corresponding to carbon bonded with nickel (denoted as C–Ni in Figure 2). The amount of C–Ni states decreases as the probing depth increases. The XPS data are consistent with the AEY NEXAFS spectrum of the annealed Ni-PCD, confirming that the Ni coating facilitates the transformation of the diamond surface upon heating, resulting in the development of a thin sp² carbon layer over the entire surface of the sample.

Figure 2: XPS C 1s spectra of PCD and Ni-PCD films after high vacuum annealing at 1100 °C, measured at excitation photon energies of a) 830 eV and b) 330 eV.

The chemical state of nickel in the annealed Ni-PCD film was elucidated using XPS and NEXAFS spectroscopies to probe the local environment of metal atoms on the surface and inside the bulk (Figure 3). The XPS Ni 3p spectrum was fitted by three

doublets, related to spin-orbit splitting into Ni $3p_{3/2}$ and Ni $3p_{1/2}$ components, separated by 1.6 eV (Figure 3a). The most intense doublet with Ni $3p_{3/2}$ component at 66.1 eV is attributed to metallic nickel [43]. The high-energy doublet with the Ni $3p_{3/2}$ component at 68.1 eV corresponds to the oxidized states of nickel (Ni–O). The appearance of these states may be due to the interaction of nickel with residual water in the vacuum chamber or with oxygen desorbed from the silicon substrate during annealing [44]. The low-energy doublet with the Ni $3p_{3/2}$ component at 65.0 eV can be referred to nickel bonded with carbon (Ni–C) [45]. The Ni–O and Ni–C doublets contribute no more than 14% to the total spectral area (with a surface content of less than 0.01 at%). The NEXAFS Ni L-edge spectra measured in TEY and AEY modes show peaks at 852.7 and 870.4 eV, corresponding to L_3 and L_2-edges (Figure 3b). According to their energy positions, the metallic nature of the nickel appears to dominate both in the bulk and on the surface of Ni-PCD after annealing [46].
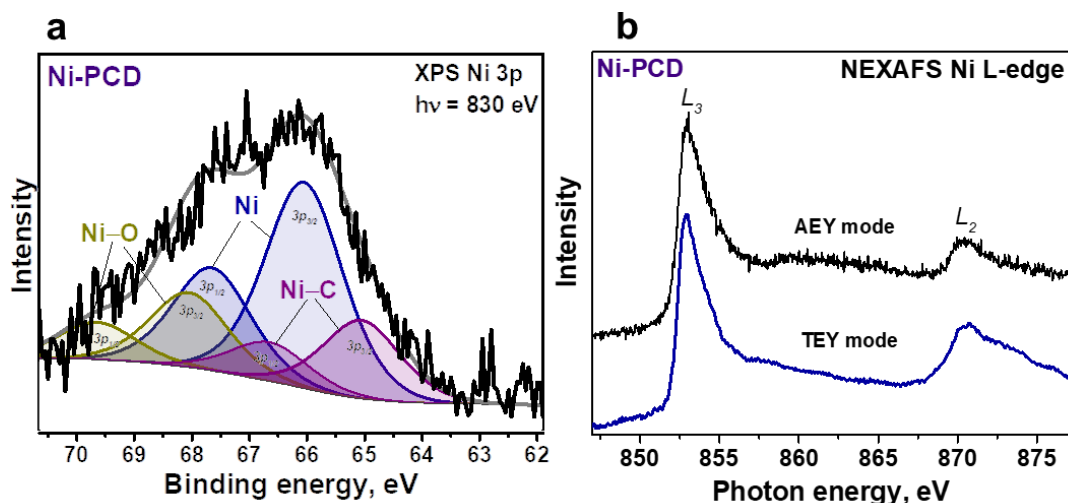
Figure 3: a) XPS Ni 3p spectrum measured at 830 eV and b) NEXAFS Ni L-edge spectra recorded in TEY and AEY modes of Ni-PCD film after high vacuum annealing at 1100 °C.

After completion of synchrotron investigations, PCD and Ni-PCD films were removed from vacuum for further SEM and Raman analysis under ambient conditions. Figure 4

shows the SEM images of some large crystallites of about 100 μm in size on the surfaces of the annealed PCD and Ni-PCD. These crystallites have well-defined triangular (111) faces and truncated rectangular faces, which could be assigned either to the (110) or (100) planes. Since the (110) orientation of grains strongly dominates, as shown by the EBSD map, the latter faces will be referred as (110). The films almost completely preserve their initial morphology after annealing. A close examination revealed that the diamond faces are flat enough and have no signs of thermal degradation. In the annealed Ni-PCD film, the crystallites have rougher surface. SEM images do not allow for a definite confirmation of whether sp^2 carbon is presented on the surface, even near defective states, partly due to its fine structure.
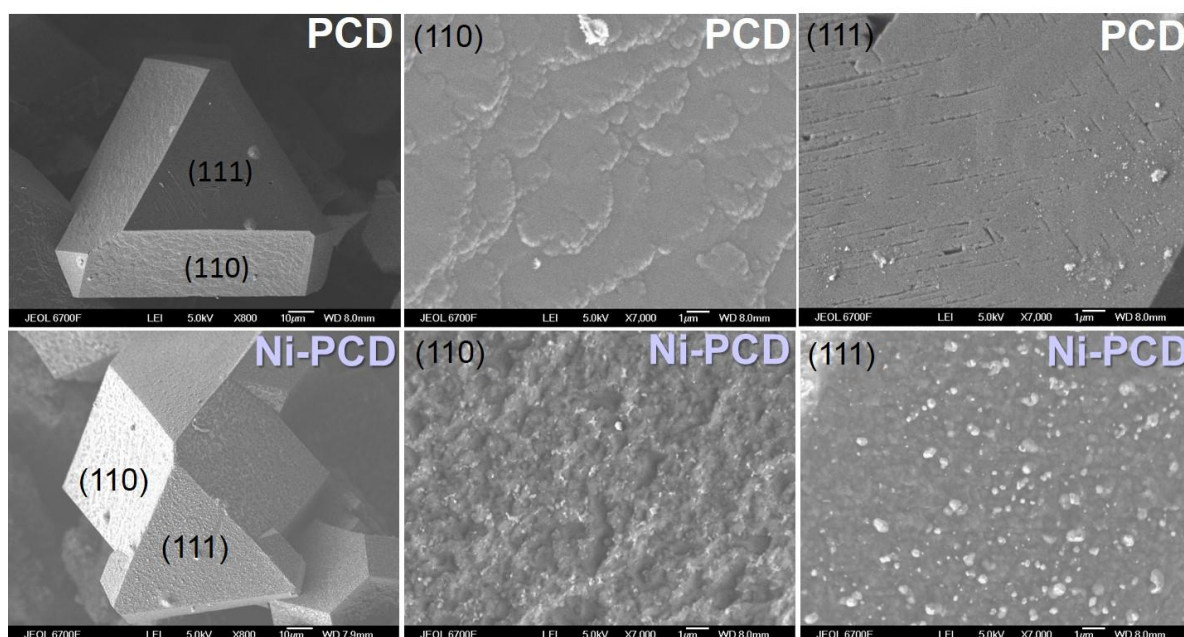
Figure 4: SEM images of the crystallites with different faces in annealed PCD and Ni-PCD films.

Comparison of SEM images taken from two different faces of the Ni-coated crystallite reveals that the nickel layer is rearranged into particles whose shape and distribution depend on the orientation of the diamond face (bright spots in bottom panels in Figure 4). In particular, on the rectangular (110) faces, nickel particles are flatter and more

evenly distributed than those on the triangular (111) face. Previous studies showed that the etching of diamond through the reaction with Ni during annealing is an anisotropic process [19, 32, 33]. In particular, the (100) and (110) faces are etched simply, while the (111) face is flattened through the process. We assume that small nickel nanoparticles formed above the (110) faces are embedded in the diamond, while their agglomerates remain on the (111) faces, appearing as large particles enclosed in carbon shells.

Raman spectroscopy was used to compare the different faces of large microcrystallites in the annealed PCD and Ni-PCD films (Figure 5 and Figure S4). Raman spectra recorded for two different faces of large microcrystallites in the annealed PCD film look similar (Figure 5a, Figure S4a,b). They demonstrate the main diamond peak at 1333 cm^{-1} corresponding to the first-order scattering of F_{2g} symmetry (Figure 5a). The high intensity and small full width at half maximum (FWHM) of 4 cm^{-1} of this diamond peak and the absence of other Raman features indicate the high crystallinity of sp^3 lattice and the low concentration of non-diamond phases in the annealed PCDs. The spectrum taken from the area between the microcrystallites, in addition to the diamond band, shows a weak Raman signal from sp^2-hybridized carbon, namely a broad G band at 1580 cm^{-1} from C=C stretching vibrations (Figure 5a). This indicates that in our experimental conditions, the partial graphitization of bare PCD film occurs more actively in the areas with small crystallites enriched with boundaries and defects, while large crystallites retains their diamond structure.

The Raman spectrum of the annealed Ni-PCD film taken from out-of-focus sample region of large area demonstrates the intense Raman peaks from both diamond and sp^2-carbon (Figure S5). In contrast to it, the Raman spectra taken from two different faces of large crystallites in the annealed Ni-PCD film and in the area with small crystallites demonstrate only the Raman peaks from sp^2-carbon and the absence of

diamond peak at 1333 cm^{-1} (Figure 5b, Figure S4c-e). The probing depth of Raman scattering is estimated to be about 90 nm (Table S1). This suggests that non-diamond components with thickness of no less than 90 nm consisting of sp^2-carbon and Raman-inactive nickel particles uniformly cover the faces of large diamond crystallites. In addition to the G band at 1584 cm^{-1}, there are two distinct peaks at 1352 and 2710 cm^{-1}, corresponding to the D and 2D bands. The D peak represents the disordered vibration modes of graphitic hexagonal layers and the 2D peak originates from the second-order double resonant scattering process. In general, the quality of graphene layers can be evaluated by the ratio of the intensities of the D and G peaks (I_D/I_G). The spectrum recorded from the area containing small diamond crystallites exhibits the highest I_D/I_G value that is twice as high as the I_D/I_G values for the faces of the large diamond crystallite. This indicates that the sp^2-hybridized carbon layers formed during the catalytic graphitization of small crystallites contain more defects compared to those formed on the continuous surface of micro-sized crystallites. The number of graphitic layers in the carbon coating forming the graphitized surface of the annealed Ni-PCD film can be analysed by the ratio of the intensity of 2D and G peaks (I_{2D}/I_G) and FWHM of the 2D peak [47]. A monolayer graphene typically has the I_{2D}/I_G values greater that 2 and a FWHM of the 2D peak of ~30 cm^{-1}. In all spectra measured from different areas of the annealed Ni-PCD film, the I_{2D}/I_G value is about 0.6 and the FWHM of 2D peak is ~90 cm^{-1}. This suggests the formation of multilayer graphitic stacks on different faces of the annealed Ni-PCD film.
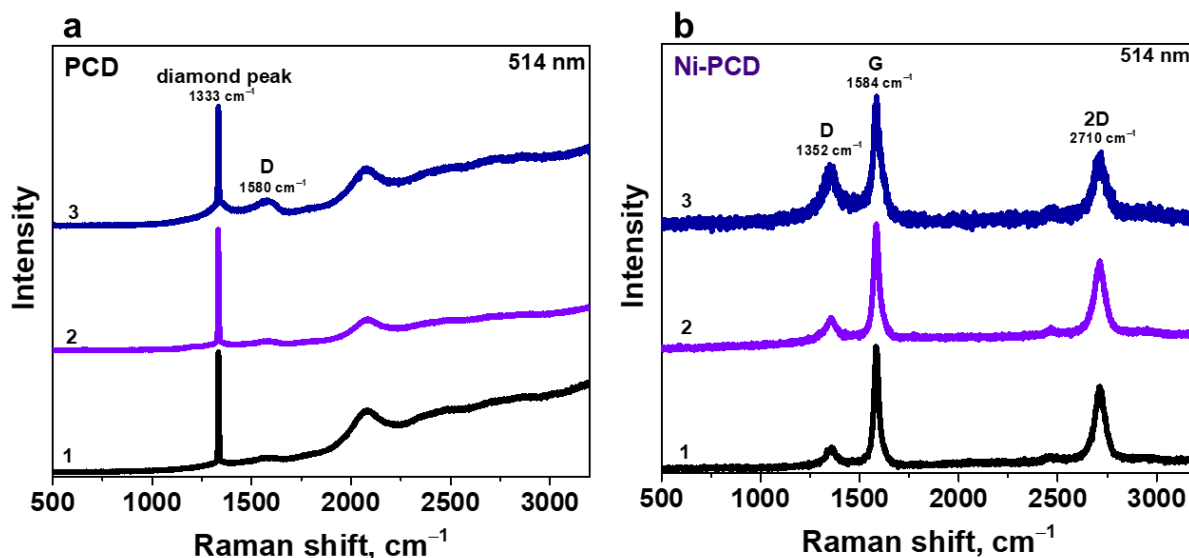
Figure 5: Raman spectra of a) PCD and b) Ni-PCD films after annealing in high vacuum at 1100 °C. The spectra were registered from two different faces of diamond microcrystal (1 and 2) and from the region between microcrystals (3).

To summarize this section, the diamond microcrystallites are highly resistant to transformation into sp^2 carbon as a result of vacuum annealing at a temperature of 1100 °C. Smaller diamond crystallites are more prone to graphitization process than large ones, and their surfaces partially transform to amorphous sp^2-like carbon. The presence of a nickel layer promotes the conversion of the diamond surface into the graphitic-like thin films with high concentration of structural defects. Although the morphology of nickel nanoparticles varies depending on the orientation of the diamond face, we do not observe differences in the chemical state of sp^2 carbon located in the same regions. This suggests that the structure of the graphitic-like coating formed during Ni-assisted graphitization depends to a small extent on the crystallographic orientation of the diamond surface and is mainly determined by the annealing temperature. On the other hand, the defectiveness of the sp^2 layers is influenced by the crystallite size and the presence of intrinsic structural defects in the diamond.

15

Orientation of graphic layers on the (110) face of single-crystal diamond after annealing at 1150 °C

In order to eliminate the role of nickel in the reconstruction of the (110) diamond surface and the orientation of sp^2 carbon layers relative to the diamond surface, we conducted angle-dependent TEY NEXAFS measurements at C K-edge of Ni-SCD after the high vacuum annealing at 1150 °C.

Figure 6 compares the C K-edge spectra of the polished (110) face of SCD (Figure 6a) and Ni-coated (110) face of SCD (Figure 6b) after annealing and subsequent cooling to room temperature. The spectra display the characteristic features of sp^3-hybridized carbon, namely, the $\sigma^*(sp^3)$-resonance at 289.3 eV and the second gap at 302.3 eV, as well as the $\pi^*(sp^2)$- and $\sigma^*(sp^2)$-resonances at 285.3 and 291.4 eV of sp^2-hybridized carbon. In the spectrum of the Ni-SCD face, the $\pi^*(sp^2)$- and $\sigma^*(sp^2)$-resonances have lower widths and significantly higher intensities (Figure 6b) compared to those in the spectra of the annealed PCD and SCD, as well as to the Ni-PCD film (Figure 1b). This data indicates that nickel facilitates the formation of the graphitic-like coating on the (110) face of SCD, which have a much more ordered graphitic-like structure than that formed on the nickel-coated polycrystalline film, in agreement with the Raman data (Figure S6).

For the annealed Ni-SCD sample, the spectra were measured at angles of 90° and 50° between the photon beam and the sample surface (Figure 6b). Changing the orientation of diamond crystal relative to the incident radiation from normal to tilted leads to a decrease in the intensity ratio of the $\pi^*(sp^2)$-resonance to the $\sigma^*(sp^2)$-resonance (I_{π^*}/I_{σ^*}). In layered graphite, there is a separation of electron orbitals with respect to symmetry: σ orbitals lie in the basal plane of graphite, while π orbitals are oriented perpendicular to this plane [48]. The difference in the polarization of π- and σ-

electrons explains the dependence of NEXAFS spectra of graphitic materials on the angle of incidence of the radiation. The decrease in the I_{π^*}/I_{σ^*} ratio with a decreasing angle between the diamond surface and the radiation indicates the predominantly vertical orientation of graphitic layers relative to the (110) diamond face [49]. A similar angular behaviour of the NEXAFS spectrum was previously observed for the iron-coated (100) face of a polished SCD after vacuum annealing at 1150 °C [26].
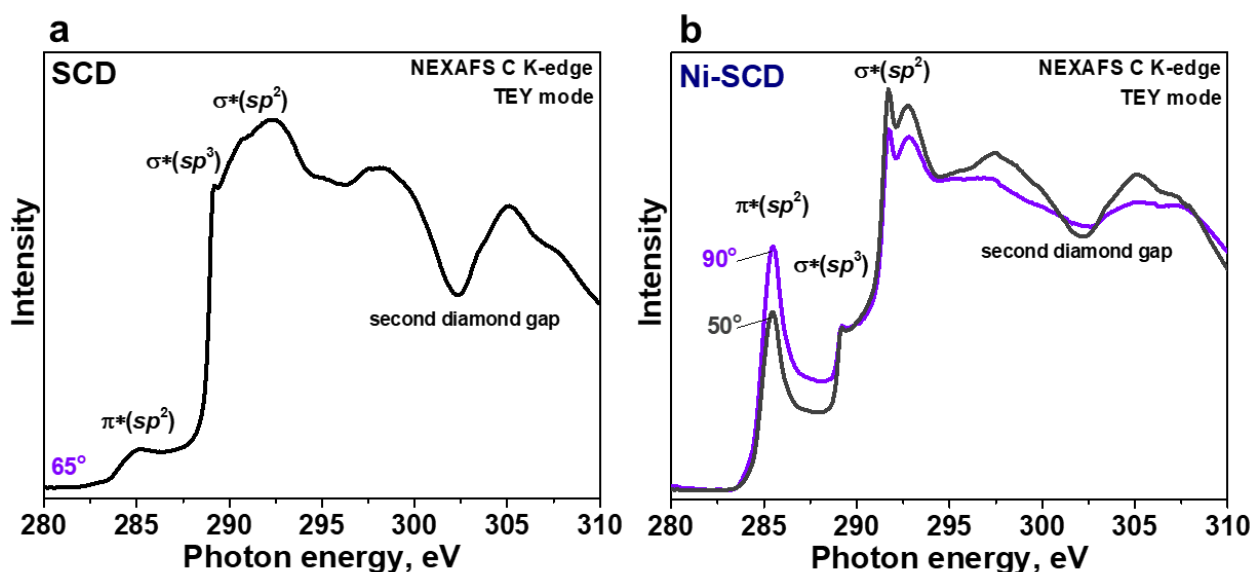
Figure 6: NEXAFS C K-edge spectra measured in TEY mode for a) bare and b) Ni-coated (110) face of SCD after annealing in high vacuum at 1150 °C. The angle of incidence of synchrotron radiation was a) 65° for SCD and b) 50 and 90° for Ni-SCD.

Conclusion

PCD films with mixed grain orientations were synthesized by the PE CVD method from acetone/methane plasma and coated with a 40-nm thick layer of nickel. In situ XPS and NEXAFS data revealed the difference in the chemical state of carbon atoms on the surface of bare and Ni-coated PCD films after annealing in high vacuum at 1100 °C. The used temperature was found to be hardly sufficient to transform the bare surface of polycrystalline film, while the presence of the nickel catalyst facilitated the

17

process, causing the formation of the graphitic-like thin coating. The SEM images revealed that nickel particles etch only the (110) face effectively, while they stay on the (111) surface, indicating anisotropic diamond etching during heating. Despite these differences, the Raman spectra recorded from the different faces of annealed microcrystallites were similar, corresponding to carbon coating composed of graphitic multilayers. This suggests that the release of sp^2 carbon from the precipitated Ni nanoparticle occurs independently on the crystallographic orientation of the diamond face. The defectiveness of sp^2-hybridized carbon layers increased in areas with fine-dispersed crystallites. The (110) face of SCD was covered with nickel, annealed in high vacuum at 1150 °C and studied using NEXAFS spectroscopy at two different angles between the diamond face and the synchrotron beam. Comparing these spectra, we observed a significant increase in the $\pi^*(sp^2)$ peak intensity with the incident angle. This behavior indicates an anisotropic texture of layered carbon coating, corresponding to the upright orientation of graphitic layers relative to the (110) face of SCD. According to this result, we suggest that multilayer graphitic layers formed on the surface of micro-sized crystallites in the annealed Ni-coated PCD are oriented perpendicular to the crystallite surface. Our results can be useful for controlling the growth of graphitic coatings on dielectric diamond surfaces with a polycrystalline structure and grains of different sizes and crystallographic orientations.

Experimental

The growth of PCD films on silicon substrates was performed using PE CVD with a hydrogen-acetone-air mixture. The deposition parameters were typical to those previously employed for an "Astex" system (2.45 GHz, 4.5 kW): a pressure of 115 Torr,

a hydrogen, acetone, and air flow rates of 500, 18, and 0.3 sccm, a substrate temperature of range 940–980 °C [27, 36]. The obtained films were about 500 µm thick. Synthetic SCD were produced using high-pressure high-temperature (HPHT) method on a BARS apparatus [49]. The starting materials included a graphite rod (99.99% purity), a $Ni_{0.7}Fe_{0.3}$ alloy as a solvent catalyst, and synthetic diamond (ca. 0.5 mm) as a seed crystal. The crystals were polished along the (110) plane to obtaine the (110)-oriented crystal substrates. The surface of a PCD film and the (110) face of a diamond crystal were coated with a nickel film using a thermal evaporation method (HBA Carl Zeiss Jena setup). The deposition parameters are described elsewhere [26]. Nickel was deposited onto the surfaces of the samples for 30 s, resulting in the formation of metallic films with a thickness of about 40 nm. The deposition region had a yellow color and was visible to the naked eye.

The thermal transformation of the samples and XPS and NEXAFS experiments were carried out at the RGL-PES end-station of the Russian-German dipole beamline (RGBL dipole) of the Berliner Elektronenspeicherring für Synchrotronstrahlung (BESSY II) operated by Helmholtz-Zentrum Berlin für Materialien und Energie (Berlin, Germany) [50]. Light polarization at RGBL dipole is linear horizontal. The samples were fixed in pairs to a molybdenum holder using molybdenum foil strips so that spectra could be recorded from bare and Ni-covered PCD films and bare and Ni-coated SDC with (110) face directed outwardly. Before measurements, the samples were annealed in ultrahigh vacuum (10^{-9} mbar) in a preparation chamber of the end-station. The annealing was performed at 1100 °C for bare and Ni-coated PCD films and at 1150 °C for bare and Ni-coated SCD samples during 15 min to reconstruct a sample surface. After annealing, the samples were cooled naturally and transferred to an analytical chamber without breaking of ultrahigh vacuum conditions.

The NEXAFS spectra of the annealed samples were registered using the total electron yield (TEY) and Auger electron yield (AEY) modes, which give complementary information about the chemical state of carbon in volume and at surface of the samples. Mean probing depth was estimated to be no more than 10 nm for TEY and 3 nm for AEY. The TEY spectra were recorded by measuring the leakage current with Kiethley ammeter. The experimental data were normalized to the ring current and photon flux measured using a clean gold crystal. In the AEY spectra, emitted Auger electrons were measured using a PHOIBOS 150 analyzer. The polar rotation of the annealed Ni-coated SCD on the manipulator was used to measure the C K-edge spectra at angles of 50 and 90° between horizontally polarized photon beam and the sample surface. The spectrum of bare SCD and PCD sample was measured at angles of 65 and 35°.

The XPS spectra were collected using the PHOIBOS 150 analyzer at photon excitation energies of 330 eV and 830 eV. Considering the electron inelastic mean free path in solids, the probing depth of XPS spectra is estimated to be approximately 3–4 nm for 830 eV and about 1 nm for 330 eV. Energy calibration of the XPS spectra was performed by referring to the Au $4f_{7/2}$ line at 84.0 eV measured from a clean Au foil. XPS data processing was carried out within the CASA XPS software Version 2.3.15. Fitting of the core-level spectra was performed using the sum of Gauss-Lorenz and Doniach-Sunjic functions after the subtraction of Shirley's background.

The morphology of the clean and Ni-coated PCD film after annealing in high vacuum at 1100 °C was studied using SEM with a JEOL 6700F microscope (accelerating voltage of 5 kV, JEOL Ltd., Tokyo, Japan). EBSD analysis of PCD crystalline orientation was performed using a Hitachi S-3400N microscope (accelerating voltage of 20 kV, Hitachi Ltd., Berkshire, UK) equipped with a HKL Advanced EBSD System Nordlys II S. The diffraction patterns were obtained by using "Flamenco" and analyzed using "Tango" software. Raman analysis was conducted

using a LabRAM HR Evolution spectrometer (Horiba Ltd., Kyoto, Japan). The spectra were excited with a 514 nm laser at a power of 1.9 mW. The laser beam was focused to a diameter of about 1 μm using an LMPlan FL 50×/0.50 Olympus objective. All measurements were carried out at room temperature.

Supporting Information

Supporting Information File 1: SM.doc

Funding

References

1. Yuan, Q.; Lin, C.-T.; Chee, K. W. A.. *APL Mater.,* **2019**, *7 (3)*, 030901.

2. Vejpravová, J. *Nanomaterials* **2021**, *11*, 2469.

3. Aitkulova, A.; Majdi, S.; Suntornwipat, N.; Isberg, J. *Phys. Status Solidi A,* **2024**, 2400567.

4. Yu, J.; Liu, G.; Sumant, A. V.; Goyal, V., Balandin A. A. *Nano Lett.* **2012**, *12 (3),* 1603–1608.

5. Zhao, F., Vrajitoarea, A., Jiang, Q.; Han, X.; Chaudhary, A.; Welch, J. O.; Jackman, R. B. *Sci. Rep.* **2015**, *5*, 13771.

6. Wu, Y., Lin, Ym., Bol, A.; Jenkins, K. A.; Xia, F.; Farmer, D. B.; Zhu, Y.; Avouris, P. *Nature* **2011**, *472*, 74–78.

7. Luo, B.; Yuan, A.; Yang, S.; Han, L.; Guan, R.; Duan, J.; Wang, C.; Dong, L.; Zhang, B.; Li, D. *ACS Appl. Nano Mater.* **2021**, *4(2)*, 1385–1393.

8. Yuan, Q.; Liu, L.; Dai, D.; Zhou, Y.; Liu, Y.; Yang, M.; Qiua, M.; Jia, Z.; Li, H.; Nishimura, K.; Tian, G.; Chee, K. W. A.; Duh, S.; Lin, C.-T.; Jiang, N.; Ouyang, X. *Functional Diamond* **2022**, *2(1)*, 94–102.

9. Seal M. *Nature.* **1960**, *185*, 522–523.

10. Bai, Q.; Wang, Z.; Guo, Y.; Chen, J.; Shang, Y. Current *Nanoscience* **2018**, *14*, 377–383.

11. Song, Y.; Larsson, K. *Advances in Nanoscience and Nanotechnology.* **2018**, *2*.

12. Enriquez, J. I. G.; Halim, H. H.; Yamasaki, T.; Michiuchi, M.; Inagaki, K.; Geshi, M.; Hamada, I.; Morikawa, Y. *Carbon* **2024**, *226*, 119223.

13. Bokhonov, B. B.; Dudina, D. V.; Sharafutdinov, M. R. Diam. *Rel. Mater.* **2021**, *118*, 108563.

14. Khmelnitsky, R. A.; Gippius, A. A. *Phase Transitions*, **2013**, 87(2), 175–192.

15. Davies, G.; Evans, T. *Proc. R. Soc. Lond. A* **1972**, *328*, 413–427.

16. García, J. M., He, R.; Jiang, M. P.; Kim, P.; Pfeiffer, L. N.; Pinczuk, A. *Carbon* **2011**, *49(3)*,1006–1012.

17. Berman, D.; Deshmukh, S.; Narayanan, B.; Sankaranarayanan, S. K. R. S.; Yan, Z.; Balandin, A. A.; Zinovev, A.; Rosenmann, D.; Sumant, Nat. A. V. Commun. **2016**, *7*, 12099.

18. Kanada, S.; Nagai, M.; Ito, S.; Matsumoto, T.; Ogura, M.; Takeuchi, D.; Yamasaki, S.; Inokuma, T.; Tokuda, N. *Diam. Rel. Mater.* **2017**, *75*, 105–109.

19. Romanyuk, O.; Varga, M.; Tulic, S.; Izak, T.; Jiricek, P.; Kromka, A.; Skakalova, V.; Rezek, B. *J. Phys. Chem. C* **2018**, *122* (*12*), 6629–6636.

20. Tulić, S.; Waitz, T.; Čaplovičová, M.; Habler, G.; Varga, M.; Kotlár, M.; Vretenár, V.; Romanyuk, O.; Kromka, A.; Rezek, B.; Skákalová, V. *ACS Nano* **2019** *13* (4), 4621–4630.

21. Tulić, S.; Waitz, T.; Čaplovičová, M.; Habler, G.; Vretenár, V.; Susi, T.; Skákalová, V. *Carbon,* **2021**, *185,* 300–313.

22. Suntornwipat, N.; Aitkulova, A.; Djurberg, V.; Majdi, S. *Thin Solid Films*, **2023**, *770*, 139766.

23. Wang, S.; Bai, Q.; Chen, S. *Cryst. Res. Technol.* **2023**, *58*, 2300122.

24. Cooil, S. P.; Song, F.; Williams, G. T.; Roberts, O. R.; Langstaff, D. P.; Jørgensen, B.; Høydalsvik, K.; Breiby, D. W.; Wahlström, E.; Evans, D. A.; Wells, J. W. *Carbon* **2012**, *50(14)*, 5099–5105.

25. Cooil, S. P.; Wells, J. W.; Hu, D.; Niu, Y. R.; Zakharov, A. A.; Bianchi, M.; Evans, D.A. *Appl. Phys. Lett.* **2015***, 107*, 181603.

26. Okotrub, A. V.; Gorodetskiy, D. V.; Palyanov, Y. N.; Smirnov, D. A.; Bulusheva, L. G. *J. Phys. Chem. C* **2023** *127* (7), 3563–3569.

27. Sedelnikova, O. V.; Gorodetskiy, D. V.; Lavrov, A. N.; Grebenkina, M. A.; Fedorenko, A. D.; Bulusheva, L. G.; Okotrub, A. V. *Synthetic Metals* **2024**, *307*, 117675.

28. Ueda, K.; Aichi, S.; Asano, H. Diam. *Rel. Mater*. **2016**, *63*, 148–152.

29. Yuan, Q.; Liu, Y.; Ye, C.; Sun, H.; Dai, D.; Wei, Q.; Lai, G.; Wu, T.; Yu, A.; Fu, L.; Chee, K. W. A. Lin, C.-T. *Biosensors and Bioelectronics* **2018**, *111*, 117–123.

30. Shen, B.; Ji, Z.; Lin, Q.; Gong, P.; Xuan, N.; Chen, S.; Liu, H.; Huang, Z.; Xiao, T.; Sun, Z. *Chem. Mater.* **2022**, *34 (9)*, 3941–3947.

31. Okotrub, A.V.; Sedelnikova, O.V.; Gorodetskiy, D.V.; Fedorenko, A.D.; Asanov, I.P.; Palyanov, Y.N.; Lapega, A.V.; Gurova, O.A.; Bulusheva, L.G. *Materials* **2023**, *16*, 1650.

32. Huang, W.-T.; Lin, C.; Li, X.; Zang, J.; Wan, L.; Zhang, Z.; Cheng, S.; Shan, C. *Acta Materialia*, **2024**, *263*, 119527.

33. Nagai, M., Nakanishi, K., Takahashi, H.; Kato, H.; Makino, T.; Yamasaki, S.; Matsumoto, T.; Inokumo, T.; Tokuda, N. *Sci. Rep.* **2018**, *8*, 6687.

34. Chen, S.; Bai, Q.; Wang, H.; Guo, W.; Dou, Y. *J. Phys. Chem. C* **2022**, *126(43)*, 18411–18420.

35. Polyakov, O. V.; Gorodetskii, D. V.; Okotrub, A. V. *Tech. Phys. Lett.* **2013**, *39*, 501–504.

36. Morar, J. F.; Himpsel, F. J.; Hollinger, G.; Hughes, G.; Jordan, J. L. *Phys. Rev. Lett.* **1985**, *54*, 1960 − 1963.

37. Sedelinikova, O.V., Gorodetskiy, D.V., Fedorenko, A.D.; Baskakova, K. I.; Paddubskaya, A. G.; Korolik, O. V.; Valynets, N. I.; Nikolenko, A. D.; Okotrub, A. V. *J Struct Chem* **65**, 1774–1783 (2024).

38. Wahab, H.; Haverkamp, R.; Kim, J. H.; Cadogan, J. M.; Mertins, H.-Ch.; Choi, S.-H.; Timmers, H. *Carbon* **2016**, *110*, 414–425.

39. Lapteva, L. L.; Fedoseeva, Y. V.; Gevko, P. N.; Smirnov, D. A.; Gusel'nikov, A. V.; Bulusheva, L. G.; Okotrub, A. V. *J. Struct. Chem.* **2017**, *58*, 1173–1179.

40. Massimi, L.; Ourdjini, O.; Lafferentz, L.; Koch, M.; Grill, L.; Cavaliere E.; Gavioli, L.; Cardoso, C.; Prezzi, D.; Molinari, E.; Ferretti, A.; Mariani, C.; Betti, M. G. *J. Phys. Chem. C* **2015**, *119*(5) 2427–2437.

41. Hwu, H. H.; Fruhberger, B.; Chen, J. G. *J. Catal.* **2004**, *221*, 170–177.

42. Tanuma, S.; Powell, C. J.; Penn, D. R. *Surf Interface Anal.* **2005**, *37*(1), 1–14.

43. Fedoseeva, Y. V.; Okotrub, A. V.; Bulusheva, L. G.; Maksimovskiy, E. A.; Senkovskiy, B. V.; Borzdov, Yu. M.; Palyanov, Yu. N. *Diam. Rel. Mater.* **2016**, *70*, 46–

44. Yamashita, T.; Hayes, P. *Appl. Surf. Sci.* **2008**, *254*, 2441–2449.

45. Lv, M.; Zhou, Y.; Rasaki, S. A.; Shen, H.; Wang, C.; Song, W.; Thomas, T.; Yang, M.; Wang,J. ChemElectroChem **2019**, *6*, 5744.

46. Ufuktepe, Y.; Akgül, G.; Aksoyc, F.; Nordlundd, D. *X-Ray Spectrometry* **2011**, *40*, 427–431.

47. Ferrari, A. C. *Solid State Commun.* **2007**, *143*, 47–57.

48. Skytt, P.; Glans, P.; Mancini, D. C.; Guo, J.-H.; Wassdahl, N.; Nordgen, J.; Ma, Y. Phys. Rev. B **1994**, *50*, 10457.

49. Belavin, V. V.; Okotrub, A. V.; Bulusheva, L. G.; Kotosonov, A. S.; Vyalykh, D. V.; Molodtsov, S. L. *J. Exp. Theor. Phys.* **2006**, *103*, 604 − 610.

50. Pal'yanov, Yu. N.; Khokhryakov, A. F.; Borzdov, Yu. M.; Sokol, A. G.; G4usev, V. A.; Rylov, G. M.; Sobolev, N. V. *Russian Geology and Geophysics*, **1997**, *38(5),* 920–945.

51. Fedoseenko, S.I.; Vyalikh, D.V.; Iossifov, I.F.; Follath, R.; Gorovikov, S.A.; Püttner, R.; Schmidt, J.S.; Molodtsov, S.L.; Adamchuk, V.K.; Gudat, W.; Kaindl, G. Nucl. *Instrum. Methods Phys. Res. A* **2003**, *505*, 718–728.